Resonant impurity and exciton states in a narrow quantum well

B. S. Monozon[1,*] and P. Schmelcher[1,2]
[1]*Theoretische Chemie, Institut für Physikalische Chemie, Universität Heidelberg, INF 229, 69120 Heidelberg, Germany*
[2]*Physikalisches Institut, Philosophenweg 12, Universität Heidelberg, 69120 Heidelberg, Germany*
(Received 23 July 2004; published 4 February 2005)

An analytical investigation of resonant impurity and exciton states in a narrow quantum well (QW) is performed. We employ the adiabatic multisubband approximation assuming that the motions parallel and perpendicular to the heteroplanes separate adiabatically. The coupling between the Coulomb states associated with the different size-quantized subbands ($N=1, 2, \ldots$) is taken into account. In the two- and three-subband approximation the spectrum of the complex energies of the impurity electron and the exciton optical absorption coefficient are derived in an explicit form. The spectrum comprises a sequence of series of quasi-Coulomb levels (n) where only the series belonging to the ground subband $N=1$ is truly discrete while the excited series $N\geqslant 2$ consist of quasi-discrete energy levels possessing non-zero widths Γ_{Nn}. Narrowing the QW leads to an increase of the binding energy and to a decrease of the resonant energy width Γ_{Nn} and the resonant energy shift ΔE_{Nn} of the impurity electron. Displacing the impurity center from the midpoint of the QW causes the binding energy to decrease while the width Γ_{Nn} and the corresponding shift ΔE_{Nn} both increase. A Lorentzian form is recovered for the exciton absorption profile. The absorption peak is narrowed and blue shifted for a narrowing of the quantum well. A successful comparison with existing numerical data is performed. For GaAs QW's it is shown that the resonant states analyzed here are sufficiently stable to be observed experimentally.

DOI: 10.1103/PhysRevB.71.085302 PACS number(s): 73.21.Fg, 73.63.Hs, 71.35.−y

I. INTRODUCTION

Since Bastard[1] and Bastard *et al.*[2] have considered the problem of an impurity electron or alternatively an exciton in the quantum well (QW) numerous experimental and theoretical papers have been published on this topic (see Refs. 3,4 and references therein). Much of this work has been devoted to the narrow QW with a width being much less than the Bohr radius of the impurity or exciton. In this case the motion of the impurity electron (exciton) possesses quasi-two-dimensional (quasi-2D) character, leading to an increase of stability. In units of the effective Rydberg constant $\mathcal{R}$ the binding energy E_b is then $E_b=4\mathcal{R}$, whereas for the bulk material we have $E_b=1\mathcal{R}$. During the last decade electronic and optical properties of nanostructures based on narrow GaAs QW of width of the order of 35 Å have become the subject of intense research.[5–8] Recently Barticevic *et al.*[9] studied theoretically excitons that are trapped by quantum defects in such a narrow QW.

In spite of the diversity of the computational methods and the strongly varying accuracy of the corresponding results on quasi-2D impurities and excitons they have a lot in common with the early pioneering works.[1,2] The absolute majority of investigations are based on numerical techniques, which employ the variational method developed originally in Refs. 1,2. However, a few investigations developed analytical approaches to the problem of the impurity[10] and exciton[11] in the QW. In these works the adiabatically slow radial motion parallel to the heteroplanes was governed by the Coulomb potential averaged with respect to the state of the Nth ($N=1, 2, 3, \ldots$) subband. A coupling between the adiabatic quasi-Coulomb radial states associated with the different size-quantized states, i.e., different N were not taken into account. In this approximation of isolated subbands, i.e., the single-subband approximation, the energies of the Coulomb interacting particle in the narrow QW consist of series of quasi-Coulomb discrete levels (n), positioned below the Nth size-quantized level and of continuous subbands (see Fig. 1). The Rydberg n states adjacent to the excited size-quantized levels $N>1$ come into resonance with the states of the continuous spectrum of lower subbands ($N-1, N-2, \ldots$) and in fact turn into so-called quasidiscrete or resonant states. The corresponding energy density consists then of peaks of finite width Γ_{Nn} determining the autoionization rate and lifetime of the resonant state.

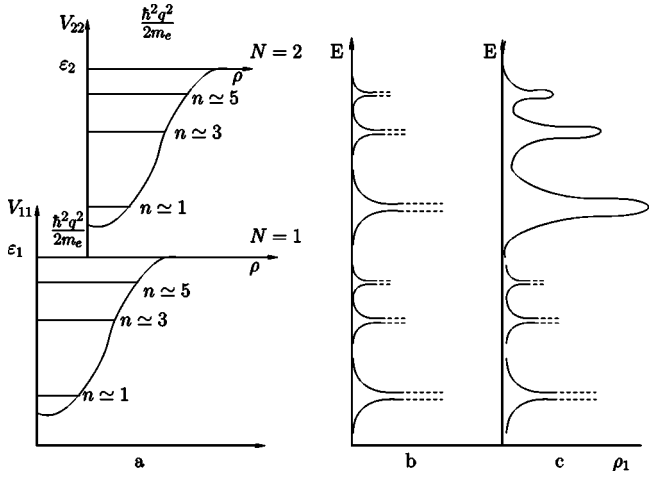

FIG. 1. (a) A schematic form of the potentials $V_{NN}(\rho)$ (6) and quasi-Coulomb discrete (n) and continuous (q) spectra (10) adjacent to the ground ($N=1$) and first excited ($N=2$) size-quantized levels $\varepsilon_N=\hbar^2\pi^2N^2/2m_ed^2$ in the the QW of width d. The density of states $\rho_\perp(11)$ is plotted as a function of the energy E (7) and (10) in the (b) single-subband (12) and (c) multisubband approximations providing the widths Γ_{Nn} (31) and (57).

At first only the discrete spectrum of the impurity and exciton states attracted attention, and subsequently the resonant states were investigated. Greene and Bajaj[12] and Fraizzoli *et al.*[13] pointed out that in a sufficiently narrow $GaAs/Ga_{1-x}Al_xAs$ QW the $2p_0$ state comes into resonance with a continuous state associated with the first subband. Using the variational approach and Dyson equation techniques Priester *et al.*[14] calculated the energy shift and width of the resonances adjacent to the third subband caused by the coupling with the first subband. Resonant states are of practical relevance since they provide a mechanism for negative differential conductance.[15] Raman scattering involving the resonant states has been observed experimentally.[16] Since localized and extended components are integrated into a common state Blom *et al.* pointed out in Ref. 17 that permanent transitions between these components and corresponding generation-recombination processes may lead to novel shot-noise parameters for devices based on the corresponding semiconductor nanostructures. The idea of population inversion of resonant states by electrically pumped carriers followed by the subsequent transition to the ground state and emission of coherent THz radiation was suggested in Refs. 18 and 4.

More recent works on resonant states in a QW are provided in Refs. 3,4 and 17. In Refs. 3 and 17 the dependencies of the binding energies and widths of the resonances on the position of the impurity and width of the GaAs/GaAlAs QW have been found numerically. Blom *et al.*[17] considered short-range and hydrogenlike impurity centers both positioned in the barrier material while Yen[3] studied impurities located within the QW. In Ref. 3 the bound part of the resonance treated as a stationary state was calculated by a variational method within the multisubband model. The extended part of the resonant states was found by a different method, namely via the resolvent operator. A comprehensive investigation of the resonant states associated with shallow donors located either outside or inside the QW was undertaken recently in Ref. 4 defining the state of the art. Particularly the binding energies and widths of the resonant states adjacent to the first excited subband ε_2 were calculated numerically for the parameters of a real Si/SiGe QW. Converting the Schrödinger equation for the total wave function into a matrix problem the resonant states for the energies $\varepsilon_1 < E < \varepsilon_2$ were found. Typically matrices of the dimension 1500 were needed to obtain results within an accuracy of about 1%.

For an almost complete list of numerical studies we refer to the references provided in Ref. 3. Basis expansions with respect to the wave functions of the free electron in the QW ignoring the Coulomb attraction were used in case of the nonvariational approaches.[4,17] In most studies the obtained results are for the ground resonant state positioned in the region bound by the first and second size-quantized levels. Main attention is paid to the moderate and wide QW's for which the lifetime of the resonant impurity states is of the order of 0.1 ps,[3,4] which is not wellsuited for an experimental study. The latter can be correctly generalized to the resonant exciton states first observed to our knowledge in an experiment by Oberli *et al.*[19] in the GaAs/AlAs double-well structure. These states have been studied by the variational[20] and various numerical methods.[21–24] The QW's of wide and moderate widths were under consideration. An analytical study of the ground and excited resonant impurity and exciton states associated with arbitrary subbands in the narrow QW's has not thoroughly been performed in the literature. However an investigation of the resonant states via analytical methods is certainly of interest because it enables the basic physics of the problem to be revealed throughout the analysis.

In order to fill the above-mentioned gap the present work provides an analytical investigation of resonant impurity and exciton states in a narrow QW. The impurity center can be positioned anywhere within the well bound by infinitely high heterobarriers. The width of the QW is taken to be much less than the Bohr radius of the impurity and/or exciton. The complete wave function is then expanded with respect to the basis formed by the one-dimensional size-quantized wave functions and the radial quasi-Coulomb wave functions describing the in-plane motion. Our method is based on the matching of the Coulomb radial wave functions and those obtained by the iteration procedure at any point of the intermediate region bound by the width of the QW and the Bohr radius. The Coulomb character of the radial wave functions allows to calculate analytically for the three- and two-subband approximation the complex energy levels of the impurity electron and the excitonic absorption coefficient, respectively. As indicated not only the ground series of the resonant impurity states adjacent to the second subband are under consideration but also those associated with the third subband. In the vicinity of the resonances the shape of the exciton peak derived from the general expression attains a Lorentzian form. In contrast to the approach used in Ref. 3 both the real and imaginary parts of the complex impurity levels and resonant shift and width of the exciton peaks are calculated in frame of a common procedure. The dependencies of the energy shifts and widths of the impurity resonant states on the width of the QW and the position of the impurity and of the exciton resonances depending on the width of the QW are obtained in explicit form. It is shown that for a narrow QW the resonant widths of the impurity and exciton states are quite small and can be observed experimentally. Our analytical results are completely in line with those obtained numerically.[3,4] Estimates of the expected experimental values are made for the parameters for the GaAs QW. We note that our aim is to elucidate the physics of the resonant impurity (exciton) states in the quantum well by deriving closed form analytical expressions for their properties. We do not intend to compete with the results of computational i.e., numerical studies.

The paper is organized as follows: in Sec. II the analytical approach based on the multisubband approximation is described. The complex energies of the impurity electron are calculated in Sec. III. A discussion of the results relevant to resonant states of the impurity electron is provided in Sec. IV. In Sec. V we discuss the absorption of light induced by the optical transitions to the resonant exciton states. Section VI contains the conclusions.

II. GENERAL THEORY

Let us define our physical setup. The z axis is chosen perpendicular to the heteroplanes of the QW. The QW is

treated as a square well of width d bounded by infinite barriers at the planes $z=\pm d/2$. The parameters relevant to the calculations are the impurity Bohr radius ($a_0=4\pi\varepsilon_0\varepsilon\,\hbar^2/m_e e^2$), the impurity Rydberg constant ($\mathcal{R}=\hbar^2/2m_e a_0^2$) and the distance of the impurity centre (b) from the midpoint of the QW at $z=0$, ε is the dielectric constant and m_e is the electron effective mass. We take the energy bands to be parabolic, nondegenerate, and separated by a wide energy gap.

In the effective mass approximation and employing cylindrical coordinates, the equation describing the impurity electron at a position $\mathbf{r}(\vec{\rho},z)$ has the form

$$\left[-\frac{\hbar^2}{2m_e}\Delta-\frac{e^2}{4\pi\varepsilon_0\varepsilon\sqrt{\rho^2+(z-b)^2}}\right]\Psi(\mathbf{r})=E\,\Psi(\mathbf{r}). \quad (1)$$

By solving this equation subject to the boundary conditions

$$\Psi(\vec{\rho},\pm d/2)=0 \quad (2)$$

the energy E and wave function $\Psi(\mathbf{r})$ can be found in principle. Equations (1) and (2) imply that some simplifications are made. The transverse effective mass $m_{\perp e}$ relating to the in-plane ρ motion and the dielectric constant ε both do not depend on the longitudinal z-coordinate. In addition to these assumptions used particularly also in Ref. 4 we take the potential barriers bounding the QW to be infinite and neglect the z-dependence of the longitudinal effective mass $m_{\|e}(z)$ then setting $m_{\|e}(z)=m_{\perp e}\equiv m_e$. We realize that the approximation of the infinite barriers is not quite justified for the narrow QW. However, we believe that the explicit and transparent results calculated by employing this approximation remain qualitatively correct for the QW of finite depth. In Sec. VI we discuss the possibility of an extension of our results to the case of a penetrable QW and different transverse and z-dependent longitudinal effective masses. Following Ref. 4 we consider only cylindrically symmetric resonance states.

The solution to Eq. (1), having the magnetic quantum number $m=0$, can be written in the form

$$\Psi(\vec{\rho},z)=\sum_{N'=1}^{\infty} f_{N'}(z)R_{N'}(\rho), \quad (3)$$

where the functions

$$f_N(z)=\sqrt{\frac{2}{d}}\sin\left[\frac{N\pi}{d}\left(z-\frac{d}{2}\right)\right], \quad N=1,2,3,\ldots \quad (4)$$

describe the longitudinal size-quantized states with the energies $\varepsilon_N=\hbar^2\pi^2N^2/(2m_e d^2)$. The transverse wave functions corresponding to the motion in the x-y plane obey the equations

$$-\frac{\hbar^2}{2m_e}\left(\frac{1}{\rho}\frac{d}{d\rho}\rho\frac{d}{d\rho}\right)R_N(\rho)+\sum_{N'=1}^{\infty}V_{NN'}(\rho)R_{N'}(\rho)=E_{\perp N}R_N(\rho), \quad (5)$$

where

$$V_{NN'}(\rho)=-\frac{e^2}{4\pi\varepsilon_0\varepsilon}\left\langle N\left|\frac{1}{\sqrt{\rho^2+(z-b)^2}}\right|N'\right\rangle \quad (6)$$

and where

$$E_{\perp N}=E-\frac{\hbar^2\pi^2N^2}{2m_e d^2}, \quad N=1,2,3,\ldots. \quad (7)$$

In Eq. (6) $\langle N|\cdots|N'\rangle$ is the matrix element calculated with respect to the functions $f_N(z)$ and $f_{N'}(z)$ [see Eq. (4)].

In the absence of the impurity center ($V_{NN'}=0$) the set (5) yields independent equations for different N. The total energy E in Eq. (7) then emerges from the sequence of the subbands formed by the branches of the continuous transverse energies $E_{\perp N}=\hbar^2q^2/(2m_e)$ ($\hbar q$ is the transverse momentum) on top of the size-quantized energy levels $N=1,2,3,\ldots$ for which $E_{\perp N}=0$. The bottom of the continuous spectra is determined by $E_{\perp 1}=0$.

It follows from Eq. (6) that in the region $\rho\gg d$

$$V_{NN'}(\rho)\simeq-\frac{e^2}{4\pi\varepsilon_0\varepsilon\rho}\left[\delta_{NN'}+O\left(\frac{d^2}{\rho^2}\right)\right]. \quad (8)$$

For a narrow QW with

$$\frac{d}{a_0}\ll 1, \quad (9)$$

the off-diagonal potentials $V_{NN'}$ ($N\neq N'$) are dominated by the diagonal terms $V_{NN}[V_{NN'}\sim(d^2/a_0^2)V_{NN}]$. In this approximation the set (5) decomposes into independent equations describing the two-dimensional (2D) impurity states governed by the quasi-Coulomb potentials $V_{NN}(\rho)$, yielding the transverse energies

$$E_{\perp N}=\begin{cases}-\dfrac{4\mathcal{R}}{(n_0+2\delta n_0)^2}, \quad n_0=1,3,5,\ldots, \quad \delta n_0(d)\sim\dfrac{d}{a_0} & \text{for } E_{\perp N}\leq 0\\ \dfrac{\hbar^2q^2}{2m_e}, \quad 0\leq q\leq\infty & \text{for } E_{\perp N}\geq 0\end{cases} \quad (10)$$

and for the density of the transverse states $\rho_\perp(E_\perp)$

$$\rho_{\perp}(E_{\perp}) = \sum_{N=1}^{\infty} \rho_N(E_{\perp N}), \tag{11}$$

where

$$\rho_N(E_{\perp N}) = \begin{cases} \dfrac{m_e}{2\pi\hbar^2}\dfrac{\exp\beta}{\cosh\beta}, \quad \beta = \pi\left(\dfrac{\mathcal{R}}{E_{\perp N}}\right)^{1/2} & \text{for } E_{\perp N} \geqslant 0 \\ \dfrac{1}{\pi a_0^2}\displaystyle\sum_{n_0=1}^{\infty} \dfrac{8\delta(E_{\perp N} + 4\mathcal{R}(n_0 + 2\delta n_0)^{-2})}{(n_0 + 2\delta n_0)^3} & \text{for } E_{\perp N} \leqslant 0 \end{cases} \tag{12}$$

Thus in the single-band approximation the total energy E consists of the sequence of series of quasi-Coulomb levels (10) adjacent on the low energy side to the size-quantized levels $N=1,2,3,\ldots$. All series except the one adjacent to the ground level $N=1$ are superimposed on the $(N-1)$ branches of the continuous spectra (10) emanating from the lower size-quantised levels. Note that the density of states (11) is a sum of δ-function type singularities (12) at the quasi-Coulomb energies (10). In other words in the single-band approximation all the quasi-Coulomb states are strictly discrete. In fact discrete energy levels persist only below the boundary of the continuous spectrum. In our case of the impurity potential given in Eq. (1) only the quasi-Coulomb series $E_{\perp 1}$ [see Eq. (10)] adjacent to the lowest boundary of the continuous spectrum $E_{\perp 1}=0$ consists of strictly discrete states $n_0=1,3,5,\ldots$. All other series adjacent to the excited size-quantized levels $N \geqslant 2$ are quasidiscrete. The reason is that the states of these series are in resonance with the states of the continuous spectrum associated with the $N-1$ subbands and lead to an autoionization process. The density of states (11) then consists of a quasi-Coulomb series of finite peaks $n_0=1,3,5,\ldots$ each determined by a nonzero width Γ_{Nn} (see Fig. 1). The latter is as usual related to the autoionization rate $\Gamma_{Nn}/\hbar$ and lifetime $\tau_{Nn}=\hbar/\Gamma_{Nn}$ of the resonant state.

Below we consider a three-band approximation describing the interaction between the quasi-Coulomb states $n_0=1,3,5,\ldots$ adjacent to the size-quantized energy levels $N=2,3$ on the one hand and the states of the continuous spectrum emanating from the size-quantized energy levels $N=1,2$ on the other hand. In this approximation the real and imaginary parts of the complex quasi-Coulomb energy levels determining the positions and widths of the peaks of the energy level density.

III. THREE-BAND APPROXIMATION—RESULTS FOR THE IMPURITY

In the three-band approximation the set of Eqs. (5) for N, $N'=1,2,3$ can be written in the form

$$\left[\frac{d^2}{dv^2} + \frac{1}{v}\frac{d}{dv} + \frac{ip}{2}V_{11}(p,v) - \frac{1}{4}\right]R_1(p,v) + \frac{ip}{2}[V_{12}(p,v)R_2(n,v) + V_{13}(p,v)R_3(\nu,v)] = 0, \quad v = \frac{4\rho}{ipa_0} \tag{13}$$

$$\left[\frac{d^2}{du^2} + \frac{1}{u}\frac{d}{du} + \frac{n}{2}V_{22}(n,u) - \frac{1}{4}\right]R_2(n,u) + \frac{n}{2}V_{21}(n,u)R_1(p,u) = 0, \quad u = \frac{4\rho}{na_0} \tag{14}$$

$$\left[\frac{d^2}{dt^2} + \frac{1}{t}\frac{d}{dt} + \frac{ik}{2}V_{22}(k,t) - \frac{1}{4}\right]R_2(k,t) + \frac{ik}{2}V_{23}(k,t)R_3(\nu,t) = 0, \quad t = \frac{4\rho}{ika_0} \tag{15}$$

$$\left[\frac{d^2}{d\tau^2} + \frac{1}{\tau}\frac{d}{d\tau} + \frac{\nu}{2}V_{33}(\nu,\tau) - \frac{1}{4}\right]R_3(\nu,\tau) + \frac{\nu}{2}[V_{31}(\nu,\tau)R_1(p,\tau) + V_{32}(\nu,\tau)R_2(k,\tau)] = 0, \quad \tau = \frac{4\rho}{\nu a_0} \tag{16}$$

In the above equations the following notations have been used:

$$V_{NN'}(n,u) = \left\langle N \left| \frac{1}{\sqrt{u^2 + g^2/n^2}} \right| N' \right\rangle, \quad g(z) = \frac{4|z-b|}{a_0},$$

$$E_{\perp 1} = \frac{4\mathcal{R}}{p^2}, \quad E_{\perp 3} = -\frac{4\mathcal{R}}{\nu^2},$$

$$E_{\perp 2}=\begin{cases}-\dfrac{4\mathcal{R}}{n^2}, & \text{for } E_{\perp 2}\leqslant 0\\ \dfrac{4\mathcal{R}}{k^2}, & \text{for } E_{\perp 2}\geqslant 0\end{cases}$$

The potentials $V_{NN'}(p,v), V_{NN'}(k,t)$, and $V_{NN'}(\nu,\tau)$ can be obtained from the potential $V_{NN'}(n,u)$ by replacing

$$u\leftrightarrow v,t,\tau \text{ and } n\leftrightarrow ip,ik,\nu, \tag{17}$$

respectively. The quantum numbers obey the relationships

$$\frac{1}{n^2}+\frac{1}{p^2}=3\left(\frac{\pi a_0}{2d}\right)^2,\quad \frac{1}{\nu^2}+\frac{1}{p^2}=8\left(\frac{\pi a_0}{2d}\right)^2,$$
$$\frac{1}{k^2}+\frac{1}{\nu^2}=5\left(\frac{\pi a_0}{2d}\right)^2. \tag{18}$$

Equations (13)–(16) are solved by matching the corresponding solutions in the region $d\ll\rho\ll a_0$. For $\rho\gg d(u,v,t,\tau\gg g)$ keeping in Eqs. (13)–(16) only diagonal terms $\sim\delta_{NN'}$ in the potentials (8) we arrive at the solutions

$$R_2(n,u)=A_2u^{-1/2}W_{n/2,0}(u), \tag{19}$$

where $W_{n/2,0}$ is the Whittaker function,[25] and A_2 is a constant. The functions $R_1(p,v), R_2(k,t)$, and $R_3(\nu,\tau)$ can be obtained from the function $R_2(n,u)$ by the replacement (17) and replacing A_2 by A_1, B_2, and A_3, respectively. The functions $R_2(n,u)$ and $R_3(\nu,\tau)$ correspond to the discrete 2D Coulomb states while the functions $R_1(p,v)$ and $R_2(k,t)$ are the functions of the continuous energy spectrum with the asymptotics of outgoing waves

$$R_1\sim A_1\exp\left[\frac{2i\rho}{pa_0}+\frac{ip-1}{2}\ln\left(\frac{4\rho}{ipa_0}\right)\right],\quad \frac{4\rho}{pa_0}\gg 1$$

In the region $\rho\ll a_0(u,v,t,\tau\ll 1)$ an iteration procedure is performed by double integration of Eqs. (13)–(16) using the trial function $R_2^{(0)}$ and its first derivative $(R_2^{(0)})'$

$$R_2^{(0)}(n,u)=c_2[\ln(u+\sqrt{u^2+g^2/n^2})+\alpha_2], \tag{20}$$

$$(R_2^{(0)}(n,u))'=c_2\left[\frac{1}{\sqrt{u^2+g^2/n^2}}-\frac{n}{g}-\frac{n}{2}\frac{u}{\sqrt{u^2+g^2/n^2}}\right.$$
$$\left.\times\ln(u+\sqrt{u^2+g^2/n^2})\right]. \tag{21}$$

The trial functions $R_1^{(0)}(p,v), R_2^{(0)}(k,t)$, and $R_3^{(0)}(\nu,\tau)$ and their corresponding first derivatives $(R_1^{(0)}(p,v))', (R_2^{(0)}(k,t))'$, and $(R_3^{(0)}(\nu,\tau))'$ can be obtained from Eqs. (20) and (21), respectively, by the replacements given in Eq. (17) and by replacing c_2 by c_1, a_2, c_3 and α_2 by $\alpha_1, \beta_2, \alpha_3$, respectively. As a result of the iteration procedure we have for $u,v,t,\tau\gg g_{NN'}$, $N, N'=1, 2, 3$

$$R_1(p,v)=c_1\left[\ln v+\alpha_1+i\frac{\pi}{2}+ip\left(\frac{1}{g_{11}}-\frac{\alpha_1}{2}\right)v\ln v\right]$$
$$-c_2\frac{g_{12}\alpha_2}{2}-c_3\frac{g_{13}\alpha_3}{2}, \tag{22}$$

$$R_2(n,u)=c_2\left[\ln u+\alpha_2+i\frac{\pi}{2}+n\left(\frac{1}{g_{22}}-\frac{\alpha_2}{2}\right)u\ln u\right]$$
$$-c_1\frac{g_{21}\alpha_1}{2}, \tag{23}$$

$$R_2(k,t)=a_2\left[\ln t+\beta_2+i\frac{\pi}{2}+ik\left(\frac{1}{g_{22}}-\frac{\beta_2}{2}\right)t\ln t\right]-c_3\frac{g_{23}\alpha_3}{2}, \tag{24}$$

$$R_3(\nu,\tau)=c_3\left[\ln\tau+\alpha_3+i\frac{\pi}{2}+\nu\left(\frac{1}{g_{33}}-\frac{\alpha_3}{2}\right)\tau\ln\tau\right]$$
$$-c_1\frac{g_{31}\alpha_1}{2}-a_2\frac{g_{32}\beta_2}{2}, \tag{25}$$

where $g_{NN'}=\langle N|g(z)|N'\rangle$.

In the region $u\ll 1$ the function $R_2(n,u)$ Eq. (19) is given by[25]

$$R_2(n,u)=-\frac{A_2}{\Gamma((1-n)/2)}\left[\ln u+\psi\left(\frac{1-n}{2}\right)+2C-\frac{n}{2}u\ln u\right], \tag{26}$$

where $\psi(x)$ is the psi function [the logarithmic derivative of the gamma-function $\Gamma(x)$] and C is the Euler constant (=0.577). The functions $R_1(p,v), R_2(k,t)$, and $R_3(\nu,\tau)$ for $v,t,\tau\ll 1$ can be obtained from Eq. (26) by the same replacements used to obtain these functions from Eq. (19). On substituting the expressions (26) for $R_2(n,u)(u\ll 1)$ and those for $R_1(p,v)(v\ll 1)$, $R_2(k,t)(t\ll 1)$, and $R_3(\nu,\tau)(\tau\ll 1)$ into the left-hand parts of the corresponding equations (22)–(25) a comparison of the coefficients is made between the results of the double integration taken for $g_{NN'}\ll u,v,t,\tau\ll 1$ and the expansions of the Whittaker functions involved particularly in Eq. (26). When terms of the same order are equated we obtain a set of four homogeneous algebraic equations for the coefficients $c_N(N=1,2,3)$, a_2. This set is solved by the determinantal method to give a transcendental equation

$$\left(\lambda_2\varphi_3-\frac{g_{23}^2}{g_{22}g_{33}}\right)\left(\lambda_1\varphi_2-\frac{g_{12}^2}{g_{22}g_{11}}\right)-\lambda_2\varphi_2\frac{g_{13}^2}{g_{11}g_{33}}=0, \tag{27}$$

where

$$\lambda_1=\frac{2}{g_{11}}-\psi\left(\frac{1-ip}{2}\right)+i\frac{\pi}{2},\quad \lambda_2=\frac{2}{g_{22}}-\psi\left(\frac{1-ik}{2}\right)+i\frac{\pi}{2},$$
$$\varphi_2=\frac{2}{g_{22}}-\psi\left(\frac{1-n}{2}\right),\quad \varphi_3=\frac{2}{g_{33}}-\psi\left(\frac{1-\nu}{2}\right).$$

A. States adjacent to the size-quantized level $N=2$

Setting in Eq. (27) $n=n_0+2\chi$, $n_0=1,3,5,\ldots$, $\chi\ll 1$, $p\simeq 3^{-1/2}(2d/\pi a_0)\ll 1$, $\nu\simeq 5^{-1/2}(2d/\pi a_0)\ll 1$, $k\simeq in$, $\varphi_3\simeq 2/g_{33}$, $\lambda_2\simeq 2/g_{22}$ and neglecting the effect of the subband

$N=3$ of the order of $d/a_0 \ll 1$ we obtain from Eq. (27)

$$\varphi_2 - \frac{g_{12}^2}{\lambda_1 g_{11} g_{22}} = 0, \tag{28}$$

where

$$\varphi_2 = \frac{2}{g_{22}} - \frac{1}{\chi}, \quad \lambda_1 = \frac{2}{g_{11}} + i\frac{\pi}{2}$$

The complex root χ of Eq. (28) determines the quantum number n and the transverse energy $E_{\perp 2} = -4\mathcal{R}/n^2$

$$E_{\perp 2}(n_0) = -\frac{4\mathcal{R}}{n_0^2} + \Delta E_{\perp 2}(n_0) - \frac{i}{2}\Gamma_2(n_0), \tag{29}$$

where

$$\Delta E_{\perp 2}(n_0) = \frac{8\mathcal{R}}{n_0^3}\left(\frac{d}{a_0}\right)\Phi_2(\varphi)\left[1 + \left(\frac{16}{3\pi^2}\right)^2\left(\frac{d}{a_0}\right)^2\Phi_{21}(\varphi)\right] \tag{30}$$

and

$$\Gamma_2(n_0) = \frac{\pi\mathcal{R}}{n_0^3}\left(\frac{32}{3\pi^2}\right)^2\left(\frac{d}{a_0}\right)^4\Phi_1(\varphi)\Phi_2(\varphi)\Phi_{21}(\varphi). \tag{31}$$

In Eqs. (30) and (31) the following notations are used:

$$\Phi_1(\varphi) = 1 + \frac{4}{\pi^2}\left[\frac{\varphi^2}{4} - \cos^2\left(\frac{\varphi}{2}\right)\right],$$

$$\Phi_2(\varphi) = 1 + \frac{1}{\pi^2}(\varphi^2 - \sin^2\varphi),$$

$$\Phi_{21}(\varphi) = \sin^2\left(\frac{\varphi}{2}\right)\left[-1 + \frac{1}{3}\sin^2\left(\frac{\varphi}{2}\right)\right]^2, \quad \varphi = \frac{2\pi b}{d}.$$

B. States adjacent to the size-quantized level $N=3$

Below we consider the resonant impurity states adjacent to the $N=3$ size-quantized level. The distinct feature of these states is their nonzero width produced by the impurity positioned at the midpoint of the QW. Note that for the resonances associated with the $N=2$ subband considered above and in Refs. 3 and 4 the width $\Gamma_2(n_0)$ (31) vanishes at $b=0(\varphi=0)$. Putting in Eq. (27) $\nu=n_0+2\zeta$, $n_0=1,3,5,\ldots$, $\zeta \ll 1$, $k \simeq 5^{-1/2}(2d/\pi a_0) \ll 1$, $p \simeq 8^{-1/2}(2d/\pi a_0) \ll 1$, $n \simeq ik$, $\varphi_2 \simeq 2/g_{22}$ we have

$$\varphi_3 - \frac{g_{32}^2}{\lambda_2 g_{22} g_{33}} - \frac{g_{31}^2}{\lambda_1 g_{33} g_{11}} = 0, \tag{32}$$

where

$$\varphi_3 = \frac{2}{g_{33}} - \frac{1}{\zeta}, \quad \lambda_2 = \frac{2}{g_{22}} + i\frac{\pi}{2}.$$

The complex root ζ of Eq. (32) determines the quantum number ν and the transverse energy $E_{\perp 3} = -4\mathcal{R}/\nu^2$

$$E_{\perp 3}(n_0) = -\frac{4\mathcal{R}}{n_0^2} + \Delta E_{\perp 3}(n_0) - \frac{i}{2}\Gamma_3(n_0), \tag{33}$$

where

$$\Delta E_{\perp 3}(n_0) = \frac{8\mathcal{R}}{n_0^3}\left(\frac{d}{a_0}\right)\Phi_3(\varphi)\left\{1 + \left(\frac{2}{\pi^2}\right)^2\left(\frac{d}{a_0}\right)^2 \times [\Phi_{32}(\varphi) + \Phi_{31}(\varphi)]\right\}; \tag{34}$$

and

$$\Gamma_3(n_0) = \frac{16\mathcal{R}}{n_0^3\pi^3}\left(\frac{d}{a_0}\right)^4\Phi_3(\varphi)[\Phi_2(\varphi)\Phi_{32}(\varphi) + \Phi_1(\varphi)\Phi_{31}(\varphi)]. \tag{35}$$

In Eqs. (34) and (35) the following notations are employed:

$$\Phi_3(\varphi) = 1 + \left(\frac{2}{3\pi}\right)^2\left[\left(\frac{3\varphi}{2}\right)^2 - \cos^2\left(\frac{3\varphi}{2}\right)\right],$$

$$\Phi_{32}(\varphi) = 4\left[\sin\left(\frac{\varphi}{2}\right) - \frac{1}{25}\sin\left(\frac{5\varphi}{2}\right)\right]^2, \quad \Phi_{31}(\varphi) = \cos^8\left(\frac{\varphi}{2}\right).$$

Equations (30) and (31) and (34) and (35) determine the corrections to the real parts $\Delta E_{\perp N}(n_0)$ of the Coulomb levels $E_{\perp}^{(0)} = -4\mathcal{R}/n_0^2$, $(n_0=1,3,5,\ldots)$ and their resonant widths $\Gamma_N(n_0)$ caused by the finite width d of the QW for the quasidiscrete states adjacent to the size-quantized levels $N=2$ and $N=3$, respectively. The corrections $\Delta E_{\perp N}(n_0)$ (30) and (34) each consists of two terms. The first terms $(\sim d/a_0)$ can be obtained in the single-subband approximation while the second ones $(\sim (d/a_0)^3)$ are the resonant impurity shifts

$$\Delta E_{\perp 2}^{(r)}(n_0) = \frac{8\mathcal{R}}{n_0^3}\left(\frac{16}{3\pi^2}\right)^2\left(\frac{d}{a_0}\right)^3\Phi_2(\varphi)\Phi_{21}(\varphi) \tag{36}$$

and

$$\Delta E_{\perp 3}^{(r)}(n_0) = \frac{8\mathcal{R}}{n_0^3}\left(\frac{2}{\pi^2}\right)^2\left(\frac{d}{a_0}\right)^3\Phi_3(\varphi)[\Phi_{32}(\varphi) + \Phi_{31}(\varphi)] \tag{37}$$

that result from the intersubband coupling.

IV. DISCUSSION OF THE RESULTS ON IMPURITIES

We define the binding energy of the impurity electron E_b as the real part of the difference between the size-quantized energy $\hbar^2\pi^2N^2/2m_ed^2$ of the free electron and the energy of the impurity electron E. It follows from Eq. (7) that

$$E_{bN}(n_0) = \frac{4\mathcal{R}}{n_0^2} - \Delta E_{\perp N}(n_0), \quad N = 2,3,\ldots, \quad n_0 = 1,3,5,\ldots, \tag{38}$$

where the energies $\Delta E_{\perp N}(n_0)$ are given by Eqs. (30) and (34) for $N=2$ and $N=3$, respectively. We observe that for the 2D layer $(d=0)E_{b2}(n_0)=E_{b3}(n_0)=4\mathcal{R}/n_0^2$ which subsequently

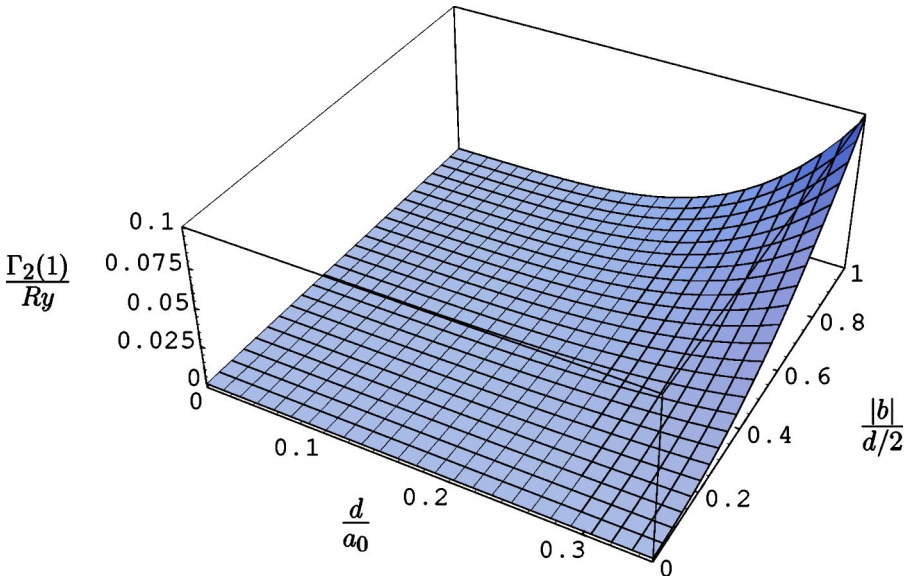

FIG. 2. The dimensionless resonant width $\Gamma_2(1)/\mathcal{R}$ (31) of the ground impurity state ($n_0=1$) adjacent to the $N=2$ subband plotted as a function of the relative impurity position $|b|/(d/2)$ and the width of the QW d ($\mathcal{R}$ and a_0 are the impurity Rydberg constant and the Bohr radius, respectively).

decreases with increasing width d. This is in agreement with the well established numerical results.[1,3,4] In the single-band approximation the contribution to a redshift of the binding energy $\Delta E_{bN}(d)$ caused by the finite width d becomes $\Delta E_{bN}(d) \sim -\mathcal{R}(n_0^{-3})(d/a_0)\Phi_N(\varphi)$, while the resonant shift resulting from the interband coupling is $\Delta E_{bN}(d) \sim -\mathcal{R}(n_0^{-3})(d/a_0)^3\Phi_N(\varphi)\Phi_{NN'}(\varphi)$.

The dependence of the binding energy E_{bN} (38) on the displacement of the impurity center b is described by the functions $\Phi_N(\varphi), \Phi_{NN'}(\varphi)$, $N=2,3$, $N'=1,2$ [see Eqs. (30) and (34)]. It follows from these equations and Eq. (38) that the binding energy decreases when the impurity shifts from the midpoint of the QW $z=0$ towards the boundaries $z=\pm d/2$. This result coincides with those calculated in Refs. 1, 4, and 26–28. To our knowledge, only Yen recently reported about the opposite dependence [see Fig.1(a) in Ref. 3).

Since the dependencies of the binding energies on the width of the QW d and the impurity position b found in the multisubband approximation coincide qualitatively with those calculated for the isolated subbands below we concentrate on the resonant widths $\Gamma_N(n_0)$ and shifts $\Delta E_{\perp N}^{(r)}(n_0)$ just caused by the intersubband coupling. It is clear from Eqs. (31) and (35) that increasing d leads to increasing widths $\Gamma_N(n_0) \sim \mathcal{R}(n_0^{-3})(d/a_0)^4$. This is similar to what has been obtained by Yen[3] and Blom *et al.*[4] The resonant shifts $\Delta E_{\perp N}^{(r)}(n_0)$ (36) and (37) increase as $\Delta E_{\perp N}^{(r)}(n_0) \sim \mathcal{R}(n_0^{-3})(d/a_0)^3$. Note that for the impurity positioned at the mid-point of the QW ($b=0$) the width $\Gamma_2(n_0)=0$. The reason for this is that the coupling between the $N=2$ and $N'=1$, 3 subbands vanishes at $b=0(g_{21}=g_{23}=0)$. If the impurity displaces from the mid-point ($b=0$) the width $\Gamma_2(n_0)$ (31) monotonically increases and reaches a maximum for the impurity positioned at the edge of the QW ($|b_m|=d/2$). Analogous dependence was obtained numerically by Yen,[3] whereas Blom *et al.*[4] report the result $|b_m|=0.7\ d/2$. The resonant width $\Gamma_2(1)$ (31) versus the QW width d and the impurity shift b is depicted in Fig. 2. The dependence of the resonant shift $\Delta E_{\perp 2}^{(r)}(n_0)$ (36) on the displacement b is qualitatively the same as that for the resonant width $\Gamma_2(n_0)$ (31) (see Fig. 3). In spite of the fact that the QW seems to be narrow it provides the strong dependence of the resonant impurity states on the position of the impurity centre within the well. Over the range $|b|$ from $d/4$ to $d/2$ (edge), the resonant shift $\Delta E_{\perp 2}^{(r)}(n_0)$ (36) and the resonant width $\Gamma_2(n_0)$ (31) increase by factors of 2.23 and 4.27, respectively. In an effort to the qualitative comparison only we extrapolate the numerical data for the maximum impurity resonant width $\Gamma_2^{(\max)}$ of the $2p_0$ state (the binding energy is $\mathcal{R}/4$) in the GaAs QW ($\mathcal{R}=5.83$ meV) of width 70 Å$\leqslant d \leqslant$400 Å (Ref. 3) to the width $d=30$ Å$(d/a_0 \simeq 0.3)$. We obtain the result $\Gamma_2^{(\max)} \simeq 0.090$ meV, that is close to the value 0.082 meV calculated from Eq. (31). The lifetime corresponding to this width is about 7 ps. Thus the resonant impurity states in narrow QW's should be observed experimentally.

The dependencies of the binding energy $E_{b3}(n_0)$ (38) and (34) and the resonant width $\Gamma_3(n_0)$ (35) and shift $\Delta E_{\perp 3}^{(r)}(n_0)$ (37) of the states adjacent to the $N=3$ subband on the width of the QW d and displacement b are qualitatively the same as those for the $N=2$ states. Equation (35) shows that the width of the resonant state adjacent to the third subband can be presented as a sum of contributions provided by the coupling of this subband to the first ($\sim\Phi_{31}$) and second ($\sim\Phi_{32}$) subbands. The same result is obtained in Ref. 3. In the region $|b| \ll d$ for which $\varphi \ll 1$, $\Phi_{32} \simeq 0$ the subband $N=1$ contributes mostly to the width $\Gamma_3(n_0)$ (35) while for $|b| \simeq d/2(\varphi \simeq \pi, \Phi_{31} \simeq 0)$ the subband $N=2$ plays a leading role. The position of the impurity b_0 at which the effects of the above mentioned subbands on the width $\Gamma_3(n_0)$ are in balance is determined by the root $\varphi_0 = 2\pi b_0/d$ of the equation

$$\Phi_2(\varphi_0)\Phi_{32}(\varphi_0) = \Phi_1(\varphi_0)\Phi_{32}(\varphi_0)$$

to give the result $\varphi_0=0.73(|b|=0.23d/2)$. The root $\varphi_0 = 0.81(|b|=0.26d/2)$ of the equation

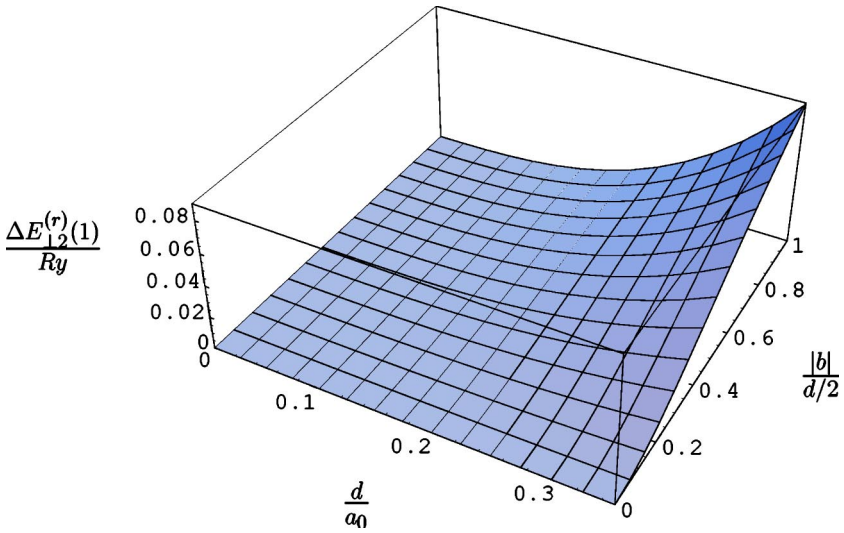

FIG. 3. The dependence of the resonant shift $\Delta E_{\perp 2}^{(r)}(1)$ (36) of the ground impurity state ($n_0=1$) adjacent to the $N=2$ subband given in terms of the impurity Rydberg constant $\mathcal{R}$ on the relative impurity position $|b|/(d/2)$ and the width of the QW d scaled to the impurity Bohr radius a_0.

$$\Phi_{32}(\varphi_0) = \Phi_{31}(\varphi_0)$$

determines the position of the impurity providing the equal contributions of the above-mentioned subbands to the resonant shift $\Delta E_{\perp 3}^{(r)}(n_0)$ (37). The contribution of the $N=1$ subband leads to resonant widths $\Gamma_3(n_0)$ (35) and shifts $\Delta E_{\perp 3}^{(r)}(n_0)$ (37) that differ from zero for any position of the impurity.

V. OPTICAL TRANSITIONS TO RESONANT EXCITON STATES

The equation describing the exciton formed by the electron (e) and hole (h) having the effective masses m_j and positions $\mathbf{r}_j(\vec{\rho}_j, z_j)$, ($j=e,h$) can be written in the form

$$\left[-\sum_{j=e,h} \frac{\hbar^2}{2m_j}\Delta_j - \frac{e^2}{4\pi\varepsilon_0\varepsilon\sqrt{(\vec{\rho}_e-\vec{\rho}_h)^2+(z_e-z_h)^2}} \right]\Psi(\mathbf{r}_e,\mathbf{r}_h) = E_{\mathrm{ex}}\Psi(\mathbf{r}_e,\mathbf{r}_h), \tag{39}$$

where $\Psi(\mathbf{r}_e,\mathbf{r}_h)$ is the exciton wave function satisfying the boundary conditions

$$\Psi\left(\vec{\rho}_e, \pm\frac{d}{2}; \vec{\rho}_h, \pm\frac{d}{2}\right) = 0, \tag{40}$$

and where E_{ex} is the total energy of the exciton.

As established[11,21,23] dipole optical transitions are allowed only to an exciton states with $N_e=N_h\equiv N=1,2,3,\ldots$, where $N_j(j=e,h)$ are the quantum numbers determining the size-quantized energy levels. Besides this, transitions are possible to the exciton states with $\mathbf{K}_\perp \simeq \mathbf{0}$ and $m=0$, where $\hbar\mathbf{K}_\perp$ is the transverse (in x-y plane of square S) momentum of the exciton and m is the magnetic quantum number. As a result the wave function $\Psi(\mathbf{r}_e,\mathbf{r}_h)$ becomes

$$\Psi(\mathbf{r}_e,\mathbf{r}_h) = \frac{1}{2\pi S}\sum_{N=1}^{\infty} f_N(z_e)f_N(z_h)R_N(\rho), \quad \vec{\rho}=\vec{\rho}_e-\vec{\rho}_h, \tag{41}$$

where the functions $f_N(z)$ are given by Eq. (4).

Substituting the wave function $\Psi(\mathbf{r}_e,\mathbf{r}_h)$ (41) into Eq. (39) we arrive at a set of equations for the radial functions $R_N(\rho)$

$$-\frac{\hbar^2}{2\mu}\left(\frac{1}{\rho}\frac{d}{d\rho}\rho\frac{d}{d\rho}\right)R_N(\rho) + \sum_{N'=1}^{\infty} V_{NN'}(\rho)R_{N'}(\rho) = E_{\perp N}^{(\mathrm{ex})}R_N(\rho). \tag{42}$$

In Eq. (42) the following notations are made

$$V_{NN'}(\rho) = -\frac{e^2}{4\pi\varepsilon_0\varepsilon}\left\langle N\left|\frac{1}{\sqrt{\rho^2+(z_e-z_h)^2}}\right|N'\right\rangle, \tag{43}$$

$$E_{\perp N}^{(\mathrm{ex})} = E_{\mathrm{ex}} - \frac{\hbar^2\pi^2N^2}{2\mu d^2} - E_g, \quad N=1,2,3,\ldots \tag{44}$$

Here $\langle N|\ldots|N'\rangle$ is the matrix element calculated with respect to the functions $f_N(z_e)f_N(z_h)$ (4), $\mu=m_em_h(m_e+m_h)^{-1}$ is the reduced effective mass of the exciton, and E_g is the forbidden gap. In Eq. (42) we keep the diagonal matrix elements (43) and only those off-diagonal matrix elements (43) providing the resonant coupling. The other matrix elements calculated with respect to the functions $f_{N_e'}(z_e)f_{N_h'}(z_h)$ (4), $N_e' \neq N_h'(N_e', N_h'=1,2)$ describing the "forbidden" exciton states, vanish because of the different parity of the "allowed" and "forbidden" exciton states (see Refs. 21 and 23 for details).

Below we consider the exciton optical absorption in the short-period QW structure[29] obeying the condition $d+D \ll 2\pi c/\omega$ where D is the width of the barriers separating the neighboring QW's and where $\omega=E_{\mathrm{ex}}/\hbar$ is the frequency of the absorbed photon. The exciton absorption is induced by the transition of an electron-hole pair from the ground state described by the function $\Psi^{(0)}(\mathbf{r}_e,\mathbf{r}_h)=\delta(\mathbf{r}_e-\mathbf{r}_h)$ to the excited state corresponding to the function $\Psi(\mathbf{r}_e,\mathbf{r}_h)$ (41). It was justified originally in Ref. 30 that the coefficient of the exciton absorption $\alpha(\omega)$ can be written in the form

$$\alpha(\omega) = \alpha_0(\omega)\Lambda(\omega), \quad \Lambda(\omega) = \frac{|R(0)|^2}{|R^{(0)}(0)|^2}, \tag{45}$$

where $\alpha_0(\omega)$ is the coefficient of the fundamental absorption associated with the free electron and hole in the conduction and valence subbands. The function $\Lambda(\omega)$ can be treated as the relative coefficient of the exciton absorption or the dimensionless density of exciton states. $R^{(0)}(\rho)$ and $R(\rho)$ are the radial wave functions of free electron-hole pair and exciton, respectively, both being normalized to the δ function $\delta(E_\perp - E'_\perp)$. Further we consider the region

$$\frac{\hbar^2\pi^2}{2\mu d^2}1^2 < (\hbar\omega - E_g) < \frac{\hbar^2\pi^2}{2\mu d^2}2^2 \tag{46}$$

bounded by the ground $N=1$ and first excited $N=2$ reduced size-quantized levels. The expression for the wave function $R^{(0)}(\rho)$ can be found from Eq. (42) for $V_{N,N'}=0$ with the result

$$R^{(0)}(\rho) = \sqrt{\frac{\mu}{\hbar^2}}J_0(q\rho), \quad q = \sqrt{\frac{2\mu E_\perp}{\hbar^2}}, \tag{47}$$

where $J_0(x)$ is the Bessel function. The exciton wave function $R(\rho)$ can be obtained by solving Eqs. (42). Since Eq. (42) can be derived from Eq. (5) by replacing m_e with μ, the averaging procedure (6) with Eq. (43) and the energy $E_{\perp N}$ (7) with the energy $E^{(\mathrm{ex})}_{\perp N}$ (44) only an outline of the corresponding calculations will be provided below.

In the two-band approximation the set of equations for the functions $R_1(\rho)$ and $R_2(\rho)$ can be derived from Eqs. (13) and (14) by taking $V_{13}=0$ and then

$$E_{\perp 1} = \frac{4\mathcal{R}^{(\mathrm{ex})}}{p^2}, \quad E_{\perp 2} = -\frac{4\mathcal{R}^{(\mathrm{ex})}}{n^2}$$

where $\mathcal{R}^{(\mathrm{ex})}=\hbar^2/2\mu a_{\mathrm{ex}}^2$ is the exciton Rydberg constant and where $a_{\mathrm{ex}}=4\pi\varepsilon_0\varepsilon\hbar^2/\mu e^2$ is the exciton Bohr radius.

Further more we employ the technique different from that providing the impurity complex energies in Sec. III. The dimensionless density of states $\Lambda(\omega)$ (45) will be found. The resonant exciton states are treated as states of the continuous spectrum with real energies. In the region $\rho \gg d$ the wave function $R_2(\rho)$ is provided by Eq. (19) with $u=4\rho/a_{\mathrm{ex}}n$ while the function $R_1(\rho)$ is taken in the form

$$R_1(p,v) = \sqrt{\frac{\mu}{\pi\hbar^2}}\exp\left(-\frac{\pi p}{4}\right)[\exp(i\Theta)v^{-1/2}W_{ip/2,0}(v) + \exp(-i\Theta)(-v)^{-1/2}W_{-ip/2,0}(-v)],$$

$$v = \frac{4\rho}{ia_{\mathrm{ex}}p}. \tag{48}$$

In the region $\rho \ll a_{\mathrm{ex}}$ we define the trial function $R_2^{(0)}(n,u)$ and its derivative $(R_2^{(0)}(n,u))'$ by Eqs. (20) and (21), respectively, while for the trial function $R_1^{(0)}(p,v)$ and its derivative $(R_1^{(0)}(p,v))'$ we take the real parts of the corresponding expressions used in Sec. III [see below Eq. (21)]. The wave functions $R_2(n,u)$ and $R_1(p,v)$ obtained by the iteration procedure can be derived from Eq. (23) and from the real part of Eq. (22), respectively by setting $c_3=0$. Then we compare these iterated functions and those obtained by the expansion of Eqs. (19) and (48) in the region $d \ll \rho \ll a_{\mathrm{ex}}$. When terms of the same order are equated we have

$$c_1 = -2\sqrt{\frac{\mu}{\pi\hbar^2}}\exp\left(-\frac{\pi p}{4}\right)\sqrt{\frac{\cosh(\pi p/2)}{\pi}} \times\cos[\Theta+\sigma(p)], \quad \alpha_N = \frac{2}{g_{NN}}, \tag{49}$$

$$c_1\left(\lambda + \frac{\pi\tan[\Theta+\sigma(p)]}{1+\exp(-\pi p)}\right) + c_2\frac{g_{12}}{g_{22}} = 0,$$

$$c_1\frac{g_{21}}{g_{11}} + c_2\varphi = 0. \tag{50}$$

Here

$$\lambda(p) = \frac{1}{2}\left[\psi\left(\frac{1+ip}{2}\right) + \psi\left(\frac{1-ip}{2}\right)\right] - \frac{2}{g_{11}}, \tag{51}$$

$$\varphi(n) = \psi\left(\frac{1-n}{2}\right) - \frac{2}{g_{22}},$$

$$\sigma(p) = \arg\Gamma\left(\frac{1+ip}{2}\right),$$

$$g_{NN'} = \frac{4}{a_{\mathrm{ex}}}\langle N|z_e - z_h|N'\rangle \ll 1, \quad N,N' = 1,2. \tag{52}$$

The set of linear algebraic equations (50) is solved by the determinantal method to give in turn the transcendental equation for the quantum numbers $n(E_{\mathrm{ex}}), p(E_{\mathrm{ex}})$ and the phase Θ

$$\varphi\left(\lambda + \frac{\pi\tan(\Theta+\sigma(p))}{1+\exp(-\pi p)}\right) - \frac{g_{12}g_{21}}{g_{11}g_{22}} = 0, \tag{53}$$

with

$$\frac{1}{n^2} + \frac{1}{p^2} = \frac{3\pi^2 a_{\mathrm{ex}}^2}{4d^2} \gg 1.$$

It follows from Eq. (20) for the wave function $R_2^{(0)}(n,u)$ and analogously for the wave function $R_1^{(0)}(p,v)$ that using Eqs. (50), (53), and (49) the exciton wave function reads

$$R(0) = R_2(n,0) + R_1(p,0) \simeq 2\left(\frac{c_2}{g_{22}} + \frac{c_1}{g_{11}}\right),$$

which yields together with Eq. (47) the analytical expression for the coefficient of the exciton absorption $\alpha(\omega)$ (45) with

$$\Lambda(\omega)=\frac{8}{\pi^2 g_{11}^2}\frac{[1+\exp(-\pi p)]\left(\varphi-\frac{g_{12}}{g_{22}}\right)^2}{\varphi^2+\frac{1}{\pi^2}[1+\exp(-\pi p)]^2\left(\frac{g_{12}^2}{g_{11}g_{22}}-\lambda\varphi\right)^2}, \tag{54}$$

where

$$g_{11}=\frac{4}{3}\left(1-\frac{15}{4\pi^2}\right)\frac{d}{a_{\mathrm{ex}}},\quad g_{22}=\frac{4}{3}\left(1-\frac{9}{16\pi^2}\right)\frac{d}{a_{\mathrm{ex}}},$$

$$g_{12}=g_{21}=-\frac{40}{9\pi^2}\frac{d}{a_{\mathrm{ex}}}.$$

The dependencies of the quantum numbers n and p as well as the functions $\varphi(n)$ (52) and $\lambda(p)$ (51) on the frequency ω are given by

$$\hbar\omega=E_g+\frac{\hbar^2\pi^2}{2\mu d^2}+\frac{4\mathcal{R}^{(ex)}}{p^2}=E_g+\frac{\hbar^2\pi^2}{2\mu d^2}4-\frac{4\mathcal{R}^{(\mathrm{ex})}}{n^2}. \tag{55}$$

Equation (54) is valid under the condition $(d/a_{\mathrm{ex}})\ll 1$ and for any frequencies in the region (46). In the limiting case of a free electron and hole ($a_{\mathrm{ex}}\to\infty$, $g_{NN'}\to 0$, $p\to 0$, $\varphi\simeq -2/g_{22}$, $\lambda\simeq -2/g_{11}$) we obtain from Eq. (54) $\Lambda(\omega)\to 1$ and the coefficient $\alpha(\omega)=\alpha_0(\omega)$, Eq. (45), describes the interband fundamental optical absorption.

VI. EXCITON SPECTRUM. RESULTS AND DISCUSSION

In the vicinity of the resonant energy $E_{\perp 2}(\nu_0)=-\mathcal{R}^{(\mathrm{ex})}/\nu_0^2$ determined by the quantum number ν_0 calculated in the single-band approximation $\varphi(\nu_0)=0$ [see Eq. (52)], Eq. (54) may be rearranged to

$$\Lambda(\omega,\nu_0)=\frac{32\mathcal{R}^{(\mathrm{ex})}}{\nu_0^3}\frac{g_{22}}{g_{11}}\times\frac{\Gamma_{\mathrm{ex}}(\nu_0)}{2\pi\{[\hbar\omega-E_{\mathrm{ex}}(\nu_0)-\Delta E_{\mathrm{ex}}(\nu_0)]^2+\Gamma_{\mathrm{ex}}^2(\nu_0)/4\}} \tag{56}$$

In Eq. (56) the following notations for the resonant width $\Gamma_{\mathrm{ex}}(\nu_0)$ and the resonant shift $\Delta E_{\mathrm{ex}}(\nu_0)$ of the resonant exciton peak both caused by the intersubband interaction are made

$$\Gamma_{\mathrm{ex}}(\nu_0)=\frac{8\mathcal{R}^{(\mathrm{ex})}g_{12}^2g_{22}}{\pi\nu_0^3g_{11}}[1-\exp(-\pi p)]\sin^2\delta, \tag{57}$$

$$\Delta E_{\mathrm{ex}}(\nu_0)=-\frac{1}{2}\Gamma_{\mathrm{ex}}(\nu_0)\cot\delta, \tag{58}$$

where

$$\cot\delta=\frac{1}{\pi}[1+\exp(-\pi p)]\lambda. \tag{59}$$

It follows from above that the exciton absorption in the short-period QW structure is reflected in the sequence of the quasi-Coulomb series of peaks marked by the quantum numbers $\nu_0\simeq 1, 3, 5, \ldots$ adjacent to the size-quantized levels $N=1, 2, 3, \ldots$ of the electron-hole pair possessing the reduced mass μ. The ground series $N=1$ consists of the σ-function type peaks for which $\alpha(\omega,\nu_0)\sim\delta(\hbar\omega-E_{\mathrm{ex}}(\nu_0))$ while the excited series $N=2, 3, \ldots$ are formed by the resonant peaks ν_0 of widths $\Gamma_{\mathrm{ex}}(\nu_0)$ shifted towards higher energies by an amount $\Delta E_{\mathrm{ex}}(\nu_0)$. The widths $\Gamma_{\mathrm{ex}}(\nu_0)$ and shifts $\Delta E_{\mathrm{ex}}(\nu_0)$ of the peaks forming the $N=2$ series are given by Eqs. (57) and (58), respectively. It follows from Eq. (55) that with narrowing the QW the exciton peaks are subject to a blue shift. This is in agreement with the results of the numerical approaches.[21,23] The optical maxima ν_0 of the excited series possess a Lorentzian form (56). Equations (57)–(59) enable us to obtain the qualitative dependencies of the optical width $\Gamma_{\mathrm{ex}}(\nu_0)$ and the shift $\Delta E_{\mathrm{ex}}(\nu_0)$ on the width d of the QW

$$p\simeq 0,\quad \lambda\simeq-\frac{2}{g_{11}},\quad \sin\delta\simeq\delta\simeq-\frac{\pi g_{11}}{4},\quad \cos\delta\simeq 1,$$

$$\Gamma_{\mathrm{ex}}(\nu_0)\simeq\frac{\mathcal{R}^{(\mathrm{ex})}}{\nu_0^3}\left(\frac{d}{a_{\mathrm{ex}}}\right)^4,\quad \Delta E_{\mathrm{ex}}(\nu_0)\simeq\frac{\mathcal{R}^{(\mathrm{ex})}}{\nu_0^3}\left(\frac{d}{a_{\mathrm{ex}}}\right)^3.$$

The relative coefficient of the exciton absorption $\Lambda(\omega,\nu_0)$ calculated from Eqs. (45) and (54) is plotted as a function of the photon energy $\hbar\omega$ in the vicinity of the ground state $\nu_0\simeq 1$ in Fig. 4. If the width of the QW d decreases the binding energy of the resonant exciton state $E_g+\varepsilon_2-\hbar\omega$ increases, the resonant width $\Gamma_{\mathrm{ex}}(1)$ decreases and the maximum value $\Lambda_{\max}(\omega,1)$ increases proportional to $\Gamma_{\mathrm{ex}}(1)\sim(d/a_{\mathrm{ex}})^4$ and $\Lambda_{\max}(\omega,1)\sim\Gamma_{\mathrm{ex}}^{-1}(1)\sim(d/a_{\mathrm{ex}})^{-4}$, respectively. The exciton peak positions associated with the transitions to the excited resonant states $\nu_0\simeq 3, 5, \ldots$ are determined by the values $s_0\simeq -0.11, -0.04, \ldots$. These peaks are much narrower compared to the peak associated with the ground state $[\Gamma_{\mathrm{ex}}(\nu_0)\simeq\Gamma_{\mathrm{ex}}(1)\nu_0^{-3}]$ and have the maximum values of the same order $[\Lambda_{\max}(\omega,\nu_0)\simeq\Lambda_{\max}(\omega,1)]$ for given width d of the QW. Each peak is slightly asymmetric (see inset in Fig. 4 corresponding to the ratio $d/a_{\mathrm{ex}}=0.3$). Taking for the heavy hole exciton in the GaAs QW the Rydberg constant $\mathcal{R}^{(\mathrm{ex})}\simeq 5.5$ meV we find that the exciton resonant life-time $\tau_{\mathrm{ex}}=\hbar/\Gamma_{\mathrm{ex}}$ in the well of width $d\simeq 30$ Å is of the order of 15 ps. Obviously the coupling between the different subbands does not destroy the stability of the exciton states in the narrow QW's. The feasibility of the spectroscopic manifestation of these states depends on the homogeneous line broadening caused by a number of mechanisms. Oberli *et al.*[19] observed in the luminescent exciton spectrum of the GaAs/AlAs double-quantum-well structure ($d_1=48$ Å, $d_2=165$ Å) at $T=4.2$ K the ground nonresonant peak of width $\Gamma=0.85$ meV and the resonant peak with the width $\Gamma\simeq 1.2$ meV. The width of the ground peak is of the same order as that of the resonant state ($\Gamma\simeq 0.70$ meV) calculated by Yen[3] for the QW of width $d=150$ Å. We therefore conclude that the contribution of these mechanisms to the total widths of the impurity and exciton states compared to the contribution provided by the resonant coupling is compa-

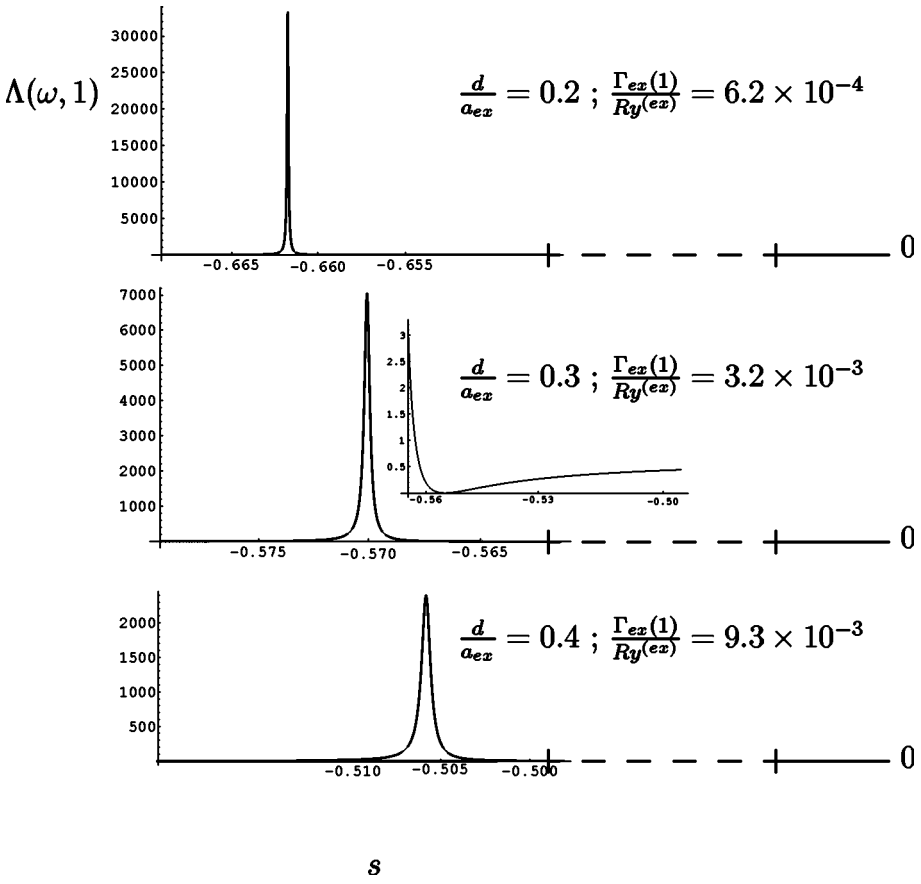

FIG. 4. The relative coefficient of the exciton absorption $\Lambda(\omega,\nu_0)$ (45) calculated from Eq. (54) for the different widths d in the vicinity of the ground peak ($\nu_0 \gtrsim 1$) (56). The parameter $s=(\hbar\omega-E_g-\varepsilon_2)/4\mathcal{R}^{(\mathrm{ex})}$ is the shift of the photon energy $\hbar\omega$ related to the edge of absorption $E_g+\varepsilon_2$ given in terms of the exciton Rydberg constant $\mathcal{R}^{(\mathrm{ex})}$.

rable in the case of moderate ($d \geqslant a_0$) QWs and significantly greater in the case of narrow ($d \ll a_0$) wells.

Our results correlate well with those derived from the Fano theory[31] taking into account the interference of a degenerate initially discrete and continuous states. Following this theory the density of the above considered exciton states in the vicinity of maxima has the Lorentzian form [the same as that given by Eq. (54)] with

$$\Gamma_{\mathrm{ex}}(\nu_0) = 2\pi|\langle R_2(\nu_0,\rho)|V_{21}(\rho)|R_1(p_0,\rho)\rangle|^2$$

and

$$\Delta E_{\mathrm{ex}}(\nu_0) = \mathrm{P}\int \frac{|\langle R_2(\nu,\rho)|V_{21}(\rho)|R_1(p,\rho)\rangle|^2}{E-E'}dE'$$

where the potential $V_{21}(\rho)$ is determined by eq. (6) and where $R_2(\nu,\rho)$ and $R_1(p,\rho)$ are the wave functions of the discrete $(\nu_0(E),\nu(E'))$ and continuous $(p_0(E),p(E'))$ spectra of the energy $E=\hbar\omega$, Eq. (55). Each peak is fitted with a shallow minimum like that given in the inset in Fig. 4. Taking for the function $R_2(\nu_0,\rho)$ in Eq. (19) $\nu_0 \simeq n=1, 3, 5, \ldots$, and normalizing it and taking for $R_1(p,\rho)$ the expression derived from Eq. (48) for $p \simeq 2d/\sqrt{3}\pi a_e \ll 1$ and from Eq. (50) for $g_{12}=0(\Theta=\pi/2)$ we immediately obtain for the width the result $\Gamma_{\mathrm{ex}}(\nu_0) \simeq (\mathcal{R}^{\mathrm{ex}}/\nu_0^3)(d/a_{\mathrm{ex}})^4$ identical to that derived from our approach. The principal part of the integral in the equation for the resonant shift $\Delta E_{\mathrm{ex}}(\nu_0)$ implies the wave function $R_1(p,\rho)$ (48) to be determined for a wide range of the quantum number $p(E')$ that requires cumbersome mathematics.

The resonant width $\Gamma_{\mathrm{ex}}(\nu_0)$ (57) and shift $\Delta E_{\mathrm{ex}}(\nu_0)$ (58) of the exciton peak coincide, respectively, with those involved in the complex energy of the exciton. This energy can be calculated employing the technique used in Sec. III [see Eq. (28)]. The roots of this equation are the same as those of the equation

$$\varphi\left(\lambda - i\frac{\pi}{2}\right) - \frac{g_{12}^2}{g_{11}g_{22}} = 0,$$

converting the denominator of Eq. (54) to zero.

As expected the width of the excitonic peak $\Gamma_{\mathrm{ex}}(\nu_0)$ and the shift $\Delta E_{\mathrm{ex}}(\nu_0)$ decrease with decreasing width d. In the single-band approximation setting in Eq. (56) $g_{12}=g_{21}=0$ we arrive at the equations

$$\Gamma_{\mathrm{ex}}(\nu_0) = \Delta E_{\mathrm{ex}}(\nu_0) = 0, \quad \Lambda(\omega,\nu_0) = \frac{32\mathcal{R}^{(\mathrm{ex})}}{\nu_0^3}\delta(\hbar\omega - E_{\mathrm{ex}}(\nu_0))$$

describing the optical absorption caused by the transitions to the strictly discrete localized exciton states.

Some remarks of general character follow. The two-subband approximation is sufficient to calculate correctly the resonant shifts $\Delta E_{\perp 2}(n_0)$ (30) and $\Delta E_{\mathrm{ex}}(\nu_0)$ (58) and the widths $\Gamma_2(n_0)$ (31) and $\Gamma_{\mathrm{ex}}(\nu_0)$ (57). The reason for this is the chosen basis comprising the radial Coulomb functions $R_N(\rho)$ of the discrete (19) and continuous spectrum. A set of plane waves $\sim\exp(i\vec{q}\vec{\rho})$ would require a considerable amount of

coupled subbands to yield similar effects. In the presented approach the localised and extended components of the resonant state are derived in a unified method in contrast to Ref. 3 where these parts are calculated employing different techniques. The dependencies of the binding energy E_{bN} (38), (30), and (34), the resonant shift $\sim(d/a_0)^3$ in Eqs. (30) and (34) and that determined by Eq. (58) and width $\Gamma_N(n_0)$ (31) and (35) and $\Gamma_{\rm ex}(\nu_0)$ (57) of the impurity electron and exciton on the width d of the QW are in complete qualitative agreement with those calculated numerically.[3,4] The fact that Refs. 3,4,20,21,23 and 24 considered moderate and wide QW's ($d>a_0$) prevents a detailed quantitative comparison with our results.

The resonant states of the Coulomb particle in the narrow QW are analogous to those in bulk material in the presence of a strong magnetic field **B**,[32,33] providing the effective two-dimensional confinement in the plane perpendicular to the magnetic field **B** bounded by the magnetic length $a_B=(\hbar/eB)^{1/2}$. The resonance comes from the coupling of the one-dimensional quasi-Rydberg and extended Coulomb states each associated with the different equidistant Landau subbands. The investigations of these diamagnetic resonant states based on the theory of Fano[31] were undertaken in Refs. 34–36 whereas the multi-subband approximation was employed in Refs. 37 and 38. Our results derived for the resonant states in the QW are in complete qualitative agreement with those corresponding to the diamagnetic resonant states in bulk material. The binding energy increases and the resonant shift and width both decrease with increase of the confinement i.e. with the decrease of the width d of the QW and the increase of the magnetic field B.

In the case of the anisotropic energy bands with the effective masses $m_{\|,\perp j}(j=e,h)$ corresponding to the motion parallel and perpendicular to the QW z axis, respectively, the impurity and exciton states depend on the ratio $m_{\perp j}/m_{\|j}$ that in principle requires a numerical study. A variational approach has shown that in bulk material and for wide QW's ($d>a_0$) for the ratio $m_{\|e}=4.63\ m_{\perp e}$ the donor binding energy is one and a half times the corresponding value for $m_{\|e}=m_{\perp e}$.[39] In a narrow QW ($d<a_0$) the in-plane motion is governed by the Coulomb potential and the effective mass $m_{\perp j}$ while the mass $m_{\|j}$ determines the z states. This allows to obtain the final results for the impurity binding energy, the exciton peak position and for the resonant shifts and widths of the impurity and exciton states by the following replacements. In Eq. (7) m_e is replaced by $m_{\|e}$, in Eqs. (29)–(31) and (33)–(38) $\mathcal{R}$ by $\mathcal{R}(m_{\perp e}/m_e)$ and a_0 by $a_0(m_e/m_{\perp e})$, in Eq. (44) μ by $\mu_\|$, and in Eqs. (54)–(56) $\mathcal{R}^{(\rm ex)}$ by $\mathcal{R}^{(\rm ex)}\mu_\perp/\mu$ and $a_{\rm ex}$ by $a_{\rm ex}(\mu/\mu_\perp)$ where $\mu_{\|,\perp}^{-1}=\mu_{\|,\perp e}^{-1}+\mu_{\|,\perp,h}^{-1}$. For a more realistic model of the QW of finite depth having the z-dependent effective masses $m_{\|eh}(z)$ the wave functions $f_N(z)$ (4) should be replaced by those relevant to the mentioned properties.[40] In particular as it follows from Ref. 41 for the QW of finite depth V under the condition $d\gg r_0$, $r_0=(\hbar^2/2\mu V)^{1/2}$ the criterion of the narrow QW (9) should be replaced by the new one $d\ll a_0-2r_0$ both for the ground $N=1$ and for the excited $N>1$ size-quantised subbands. In Ref. 3 the parameters for the GaAs QW were taken to be $V\simeq 188$ meV, $r_0\simeq 17.5$ Å, $a_0\simeq 98$ Å. Clearly the QW of width $d\simeq 30$ Å is not the best candidate of a narrow well providing the 2D character of the impurity states. As a result the $2p_0$ state considered by Yen[3] in such a well attains significantly the 3D state with the effective Rydberg constant $\mathcal{R}/4$. Consequently only a qualitative agreement between the numerical data of Yen[3] and our analytical results can be achieved. Moreover the finite depth V and the electron density related to the quasi-3D $2p_0$ state could contribute to the discrepancy between the dependencies of the binding energy on the position of the impurity obtained by Yen[3] and those calculated in this paper. However the new criterion for a narrow QW of finite depth is satisfied much better for the $Ga_{0.47}In_{0.53}As/Al_{0.48}In_{0.52}As$ QW having the parameters $V\simeq 450$ meV, $r_0\simeq 14.7$ Å, $a_0\simeq 184$ Å (Ref. 42) and $d\simeq 40-50$ Å. Thus we believe that our analytical method can be applied to the resonant impurity states in the narrow QWs of realistic width and finite depth.

Along the barriers of finite height the image charges caused by the difference between the dielectric constants of the well and barrier materials influence the impurity and exciton states. The effect of the dielectric-constant mismatch has been comprehensively studied by Fraizzoli *et al.* in Ref. 13 in which the binding energy of the impurity in the $GaAs/Ga_{1-x}Al_xAs$ QW was calculated as a function of the width of the QW and the impurity position for the Al composition $x=0.3$, 0.4. For the relative correction to the binding energy of the on-center impurity the result $\Delta E_b/E_b\sim 0.22x$ was found. On extrapolating the data obtained in Ref. 13 to the concentration $x=0.2$ taken by Yen[3] and width $d=30$ Å we find the results $\Delta E_b/E_b\simeq 5.7\%$ and $\Delta E_b/E_b\simeq 6.4\%$ for the impurity positioned at the midpoint of the QW $b=0$ and shifted towards the edge of the QW by a distance $b=d/4$, respectively. Note that the correction to the binding energy associated with the dielectric-constant mismatch remains less than that provided by the finite depth of the QW. The presented method can be extended to the case of an external electric field directed perpendicular to the heteroplanes. The matrix elements g_{ij} are calculated then with respect to the wave functions of the electron (hole) in the QW subjected to the electric field **F** $f_N(F,z)$ (Ref 43) instead of $f_N(z)$ (4) used in this paper. For the QW of intermediate width comparable to the impurity or exciton Bohr radius the two- or three-subband approximations become inappropriate. Nevertheless the resonant states can be found in the multisubband approximation. Only at the final stage of the determinantal procedure some minor numerical study is necessary. We expect that in the multisubband approximation the series (3) and (41) are rapidly convergent as happens with the series describing the diamagnetic resonant states.[38] However these states demonstrate that the multi-subband approximation[38] does not lead to significant qualitative changes relative to the two-subband model.[37]

VII. CONCLUSIONS

We have developed an analytical approach to the problem of the resonant states of an impurity electron and exciton in a narrow QW. The resonant character is caused by the intersubband coupling of the states treated as strictly discrete and extended in the single-subband approximation. The three-

and two-subband approximations are sufficient to obtain the complex energies of the impurity electron and the coefficient of the exciton absorption in explicit form. The wider the QW is the larger are the widths both of the impurity energy levels and the exciton peaks and the less are the impurity and exciton binding energies. As the impurity center shifts from the midpoint of the QW, the binding energy of the impurity electron decreases and the width of the energy level increases. With an increase of the width of the narrow QW the effect of the displacement of the impurity becomes more pronounced. Our analytical results are in complete agreement with those calculated previously numerically. Estimates of the expected values associated with the GaAs QW's show that for narrow wells we expect the resonant impurity and exciton states to be observable experimentally. The presented results can easily be extended to the case of an external electric field directed perpendicular to the heteroplanes. In principle our approach is appropriate for QWs of finite depth and moderate width comparable to the impurity or exciton Bohr radius.

ACKNOWLEDGMENT

The authors are grateful to V. Bezchastnov for valuable discussions and P. Drouvelis as well as I. Solov'ev for technical assistance. Financial support by the Deutsche Forschungsgemeinschaft is gratefully acknowledged.

*Permanent address: Department of Physics, State Marine Technical University, 3 Lotsmanskaya Str., 190008 St. Petersburg, Russia.

[1] G. Bastard, Phys. Rev. B **24**, 4714 (1981).
[2] G. Bastard, E. E. Mendez, L. L. Chang, and L. Esaki, Phys. Rev. B **26**, 1974 (1982).
[3] S. T. Yen, Phys. Rev. B **66**, 075340 (2002).
[4] A. Blom, M. A. Odnoblyudov, I. N. Yassievich, and K. A. Chao, Phys. Rev. B **68**, 165338 (2003).
[5] K. Brunner, U. Bockelmann, G. Abstreiter, M. Waltner, G. Böhm, G. Trönkle, and G. Weimann, Phys. Rev. Lett. **69**, 3216 (1992).
[6] A. Zrenner, L. V. Butov, M. Hagn, G. Abstreiter, G. Böhm, and G. Weimann, Phys. Rev. Lett. **72**, 3382 (1994).
[7] D. Gammon, E. S. Snow, B. V. Shanabrook, D. S. Katzer, and D. Park, Phys. Rev. Lett. **76**, 3005 (1996).
[8] W. Heller, U. Bockelmann, and G. Abstreiter, Phys. Rev. B **57**, 6270 (1998).
[9] Z. Barticevic, M. Pacheco, C. A. Duque, and L. E. Oliveira, Phys. Rev. B **68**, 073312 (2003).
[10] A. G. Zhilich, Sov. Phys. Solid State **33**, 158 (1991).
[11] Al. L. Efros, Sov. Phys. Semicond. **20**, 808 (1986).
[12] R. L. Greene and K. K. Bajaj, Phys. Rev. B **31**, 4006 (1985).
[13] S. Fraizzoli, F. Bassani, and R. Buczko, Phys. Rev. B **41**, 5096 (1990).
[14] C. Priester, G. Allan, and M. Lannoo, Phys. Rev. B **29**, 3408 (1984).
[15] F. Bassani, G. Ladonisi, and B. Preziosi, Rep. Prog. Phys. **37**, 1099 (1974).
[16] T. A. Perry, R. Merlin, B. V. Shanabrook, and J. Comas, Phys. Rev. Lett. **54**, 2623 (1985).
[17] A. Blom, M. A. Odnoblyudov, I. N. Yassievich, and K. A. Chao, Phys. Rev. B **65**, 155302 (2002).
[18] M. A. Odnoblyudov, I. N. Yassievich, M. S. Kagan, Yu. M. Galperin, and K. A. Chao, Phys. Rev. Lett. **83**, 644 (1999).
[19] D. Y. Oberli, G. Böhm, G. Weimann, and J. A. Brum, Phys. Rev. B **49**, 5757 (1994).
[20] A. Pasquarello and L. C. Andreani, Phys. Rev. B **44**, 3162 (1991).
[21] A. R. K. Willcox and D. M. Whittaker, Superlattices Microstruct. **16**, 59 (1994).
[22] R. Winkler, Phys. Rev. B **51**, 14 395 (1995).
[23] S. Glutsch, D. S. Chemla, and F. Bechstedt, Phys. Rev. B **51**, 16 885 (1995); **54**, 11 592 (1996)
[24] K.-I. Hino, Phys. Rev. B **64**, 075318 (2001); **62**, R10 626 (2000)
[25] *Handbook of Mathematical Functions*, edited by M. Abramowitz and I. A. Stegun (Dover, New York, 1972), p.505.
[26] C. Mailhiot, Y.-C. Chang, and T. C. McGill, Phys. Rev. B **26**, 4449 (1982).
[27] K. Tanaka, M. Nagaoka, and T. Yamabe, Phys. Rev. B **28**, 7068 (1983).
[28] R. L. Greene and K. K. Bajaj, Phys. Rev. B **31**, 913 (1985).
[29] L. E. Vorob'ev, E. L. Ivchenko, D. A. Firsov, and V. A. Shalygin, *Optical Properties of Nanostructures* (in Russian) (Nauka, St. Petersburg, 2001), p. 123.
[30] R. J. Elliot, Phys. Rev. **108**, 1384 (1957).
[31] U. Fano, Phys. Rev. **124**, 1866 (1961).
[32] R. J. Elliott and R. Loudon, J. Phys. Chem. Solids **15**, 196 (1960).
[33] H. Hasegawa and R. E. Howard, J. Phys. Chem. Solids **21**, 179 (1961).
[34] B. S. Monozon and A. G. Zhilich, Sov. Phys. Semicond. **2**, 150 (1968).
[35] S. D. Beneslavskii, Sov. Phys. Solid State **10**, 2503 (1969).
[36] E. I. Rashba and V. M. Edelstein, Sov. Phys. JETP **31**, 765 (1970).
[37] A. G. Zhilich and O. A. Maksimov, Sov. Phys. Semicond. **9**, 616 (1975).
[38] A. G. Zhilich and B. K. Kyuner, Sov. Phys. Semicond. **15**, 1108 (1981).
[39] C. Hamaguchi, *Basic Semiconductor Physics* (Springer, Berlin, 2001), p.74.
[40] P. Harrison, *Quantum Wells, Wires and Dots* (Wiley, New York, 2000), p.43.
[41] B. S. Monozon, Superlattices Microstruct. **29**, 17 (2001).
[42] Y. T. Yip and W. C. Kok, Phys. Rev. B **59**, 15 825 (1999)
[43] S. T. Giner and J. L. Gondar, Physica B & C **138**, 287 (1986).